1

Introduction and Overview of the Book

Rebecca Seviour

University of Huddersfield, School of Computing and Engineering, Queensgate, Huddersfield HD1 3DH, UK

1.1 Introduction

High-power microwaves (HPMs), or directed energy RF, is an evolution of vacuum electron devices (VEDs) that seeks to generate the highest peak power levels in the frequency range of 100 s MHz through 100 GHz (and even higher frequencies) in short pulses (10–100 s ns in duration) that can be repetitively pulsed [1, 2]. They came onto the scene in the late 1960s following the advent of pulsed power drivers that not only provided high-energy electron beams (in the order of a MeV and higher), but concomitantly provided high currents as well (1–10's kA) [3]. Similar to VEDs, the electron beam is the power source from which the microwaves grow. Unlike VEDs, HPM sources have much less-stringent vacuum and material requirements since their applications tend to be limited in scope with short mission times.

The state-of-the-art in the practice of HPM sources has been led by intense beam-driven oscillators whose output scale as Pf^2, where P is the peak output microwave power and f is the operating frequency [2, 4]. This is the Figure-of-Merit (FOM) for HPM oscillators. The equivalent FOM for HPM amplifiers is $Pf\Delta f$ where Δf is the bandwidth (BW). Until recently, conventional wisdom suggested that for emerging defense applications, the highest power on target (highest intensity field) was of greatest utility. However, recent advances in the understanding of the interaction of intense microwave fields with components and circuits argue that a tailored waveform synthesized at low power and amplified to very high power, might provide even superior capabilities. This is termed waveform diversity. Consider a comparison of the state-of-the-art oscillator and amplifier in terms of the FOM: (i) the ITER/DIII-D's plasma-heating gyrotron oscillator at 110 GHz, 1 MW (10 s pulse), 1.1 MHz BW, has a FOM 1.2×10^{12} W-GHz^2 and essentially no BW. (ii) Haystack radar's gyrotron amplifier at 94 GHz, 55 kW output power (5.5 kW average), 1600 MHz BW yields a FOM 8.3×10^6 W-GHz^2. Thus, there is a 2 order-of-magnitude opportunity to advance the FOM in high-power amplifiers with considerable BW.

Interest in metamaterials (MTMs) grew rapidly following the publication of Pendry [5] and its practical implementation by Smith afterwards [6]. As discussed in this chapter, the history of MTMs dates back to the nineteenth century with numerous contributors, many of whom have only recently been rediscovered. This history has been reviewed in several books [7, 8] and continues to be unraveled.

While numerous books have been written on the EM properties of MTMs, all of the applications that have been described in these books to-date are at low-power levels. In this book, we

High Power Microwave Sources and Technologies Using Metamaterials, First Edition.
Edited by John Luginsland, Jason A. Marshall, Arje Nachman, and Edl Schamiloglu.

bring together advances that have been made in studying MTMs as slow-wave structures (SWSs) for active electron beam-driven HPM devices. We discuss structures that satisfy Wasler's definition of a MTM (see Section 1.2), and we also describe periodic SWSs with degenerate band edges (DBEs) that do not satisfy this definition, yet do offer novel engineered dispersion relations that are relevant to our overall goal-seeking to discover novel beam/wave interactions that can be exploited for new HPM amplifiers.

1.2 Electromagnetic Materials

In many VEDs, the particle wave interaction is mediated in part via a material, where the functionality of the material manipulates the electromagnetic (EM) wave in a controlled fashion. The creativity of engineers to construct new devices is largely limited by the EM properties of available materials and the ability to precision engineer geometries from these materials. Of course, we are not restricted to naturally occurring materials; for decades, RF engineers have used materials synthesized at the molecular level with peculiar RF properties, such as Polytetraflufoethylene (Teflon™) and HfO_2. These molecular synthesized materials can be used in VEDs to modify the behavior of an EM wave in a useful manner. In a simplistic form, this behavior between wave and material is described via the constitutive relations:

$$\begin{aligned}\mathbf{D}(k,\omega) &= \epsilon(k,\omega)\mathbf{E}(k,\omega)\\ \mathbf{B}(k,\omega) &= \mu(k,\omega)\mathbf{H}(k,\omega).\end{aligned} \tag{1.1}$$

Here the permittivity (ϵ) and the permeability (μ) are the complex averaged EM response functions of the molecules that make up the material due to the interaction with the electric and magnetic components of an incident wave. The molecules in the material respond to the incident EM wave by forming dipoles, and these individual responses are averaged over all molecules in a volume $\approx \lambda^3$ to yield the permittivity and permeability. This averaging process discussed further in Section 1.3 even holds for gases as the number of molecules is still large enough that the parameters ϵ and μ accurately describe the interaction of an EM wave well into ultraviolet frequencies.

As ϵ and μ are the primary parameters that define a materials response to an EM wave it is useful to categorize materials based on the real components of these two parameters, as shown in Figure 1.1. Materials in the upper right quadrant of Figure 1.1 are often termed Double Positive Media (DPM), common dielectric materials, such as Polytetraflufoethylene, Al_2O_3. The upper-left and lower-right quadrants of Figure 1.1 are the single negative media, such as plasmas or metals with a negative permittivity and negative permeability materials such as "wet" ice crystals. Unlike the DPM these single-negative media only allow evanescent wave transport. The lower-left quadrant of Figure 1.1 represents a special case of materials where both permittivity and permeability are simultaneously negative. These Double Negative materials (DNGs) like their double-positive counterparts support wave propagation though the media. The key difference between the DNG quadrant and the other three is that single-negative and double-positive media all occur naturally, whereas we are yet to find a naturally occurring DNG media.

Although presenting fantastic opportunities, molecular synthesized materials are limited in the range of RF properties they can produce due to the nature of the EM interaction with the molecules of the material. An interaction where the light-mass negatively charged electrons surrounding the relatively large-mass positively charged nucleus of the atoms move in response to an EM wave forming a dipole. This response is fixed by both the fundamental properties (charge, mass) and the chemical bonds formed in the material, limiting the available parameter range ϵ and μ these

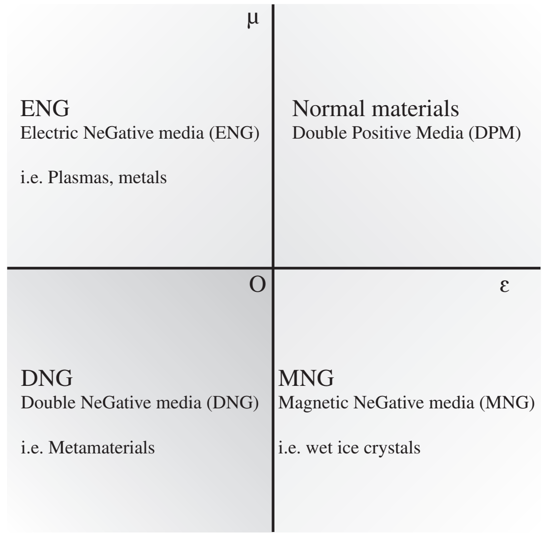

Figure 1.1 Broad categorization of materials based on the real components of the permittivity and permeability.

materials can access. These limitations have led scientists and engineers to create a range of artificial composite structures with periodic subwavelength functional inclusions. Although these inclusions are many orders of magnitude larger than the molecules of the constitutive materials, they are still much smaller that the EM wavelength of interest. In this case, to an incident EM wave, these inclusions respond no differently than giant molecules with a very large polarizability. This enables the interactions between wave and the collective structures to be described in terms of the "homogenized" abstracted bulk material parameters permittivity and permeability. Treating the collective periodic structures in this homogenized manner is called an "effective" medium or material. This approach in theory allows the engineer to fabricate artificial effective materials with specific engineered EM properties, most notable of which is the creation of the above DNG materials. There are of course restrictions on achievable physical material properties that are impossible to engineer, such as the creation of media where waves propagate with group velocities greater than the speed of light in vacuum.

Around 20 years ago, the word "MTM" entered the lexicon to refer to certain types of effective media. Even though a large number of peer-reviewed papers using the word "MTM" have been published an agreed definition of what a MTM is remains elusive. The origin of the word "meta" from the Greek "beyond" implies in some sense that "metamaterials" are a form of material beyond conventional materials. Sources suggest the term "MTM" was first coined by Rodger Walser in 1999 [9], who defined a MTM as; "*. . . macroscopic composites having man-made, three-dimensional, periodic cellular architecture designed to produce an optimized combination, not available in nature, of two or more responses to specific excitation*." Whereas the Metamorphose Network defines a metamaterial as "*. . . an arrangement of artificial structural elements, designed to achieve advantageous and unusual electromagnetic properties*" [10].

This later definition although encompassing the Walser definition could be considered too "broad," as, for example it does not recognize the critical differences between MTMs, photonics structures, and other man-made structures such as multi-input, multi-output (MIMO) antenna arrays. To quote Cai and Shalaev [8]; "*Metamaterials are, above all, man-made materials. The structural units of a metamaterial, known as meta-atoms or metamolecules, must be substantially smaller than the wavelength being considered, and the average distance between neighboring metaatoms is also subwavelength in scale. The subwavelength scale of the inhomogeneities in a metamaterial* *makes the whole material macroscopically uniform, and this fact makes a metamaterial essentially a material instead of a device. The scale of the inhomogeneities also distinguishes metamaterials from many other electromagnetic media*." These last two sentences from Wei are critical in defining the underlaying physics that enables us to consider MTMs as "effective media." For example some definitions would allow the eye of a lobster to be defined as a MTM, even though the structure of the lobster's eye works on reflection with a periodicity of ≈10 μm [11], many times larger than the wavelength of light entering the lobster eye meaning that the system cannot really be treated as an effective media.

1.3 Effective-Media Theory

Effective media theory builds upon the theoretical framework developed in the nineteenth century by Mossitti [12] and Clausius [13] on the homogenization of materials. For example consider a system of small, subwavelength, particles arranged into a lattice. If the particles are small enough, then the response of the system to an EM wave is the same as if the system were a collection of molecules with a large polarizability, i.e. if the scale of the inhomogeneities is small compared to the incident wavelength, then the system appears homogeneous to the wave. This homogenization approach allows us to predict the EM behavior of a heterogeneous system by evaluating the effective permittivity and permeability of a macroscopically homogeneous medium. Where the effective permittivity and permeability of the bulk material is found in terms of the permittivities, permeabilities, and geometry of the individual constituents of the system. This approach is the basis for many "effective media" theories, Lakhtakia [14] presents a comprehensive review of the early work on effective media theories and a review of more modern work can be found in the paper by Belov and Simovski [15] that also discusses the homogenization of MTMs including a radiation term.

Two commonly used effective media theories that illustrate the general approach are the Maxwell–Garnett [16] and the Bruggeman [17] approach. Each approach is based upon slightly different assumptions about the topology and material properties of the constituent materials. In the Maxwell–Garnett approach it is assumed that the inclusions are well-defined spheres sparsely scattered across the host medium. The Bruggeman approach is essentially a percolation approach, where the two mediums are equally intermingled. These examples highlight a key point about effective-media theories. As the effective-permittivity/permeability are averaged differently in each model, different effective-media theories cannot be directly compared to each other even when the same subwavelength configuration is considered.

1.4 History of Effective Materials

1.4.1 Artificial Dielectrics

The realization of artificial materials began a hundred years before the term "metamaterial" was introduced, with the work of Rayleigh and Bose in the 1890s. Rayleigh proposed a system of small scatterers as an equivalent continuous medium [18], and Bose produced an artificial chiral material by twisting "jute" root [19]. This work was extended in 1914 by Lindman who considered small wire helices embedded into a host medium to create an artificial chiral material [20]. The first practical applications did not appear until the 1940s with the pioneering work of Kock [21]. Kock created Artificial Dielectrics from arrays of subwavelength metallic structures (spheres, rods, and plates)

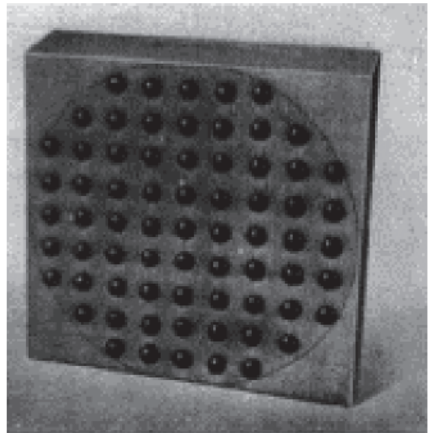

Figure 1.2 Kock's artificial dielectric lens, consisting of conducting spheres embedded in a low index foam, taken from [21]. Source: Kock [21] / with permission of John Wiley & Sons, Inc.

to form Dielectric Lenses [21] of the form shown in Figure 1.2, with the aim to develop light weight RF lens compared to their metal counterparts.

In 1953 Brown [22] extended the work of Kock, considering a lattice of thin metallic wires, showing the system could be considered to have a plasma frequency. Brown demonstrated that the system formed an artificial plasma and could be considered an effective medium with negative permittivity. In the case of lossless wires, the wire array can be modeled as an array of inductors with inductance L. In this case, the effective permittivity (ϵ_{eff}) of the system becomes

$$\epsilon_{\text{eff}}(\omega) = 1 - \frac{1}{d^2\omega^2\epsilon_o L}. \tag{1.2}$$

Importantly, Kharadly and Jackson [23] generalized this work to consider effective media formed from lattices of metal ellipsoids, disks, and rods, with the assumption that the frequency of operation is low and the Rayleigh quasi-static restriction holds. Interest in this type of effective medium grew as the possibilities for exploitation were realized, most comprehensively by Rotman [24], who explored these artificial materials as plasma analogs to investigate the effect of plasmas on antenna systems. This type of wire array media have been turned into an "active" material by the inclusion of diodes enabling the media to be actively switched from a negative to a positive permittivity medium. Progress with this type of media resulted in the material becoming commercially available in the 1970s [25]. Even today wire-array based media are still attracting interest as subwavelength elements for epsilon negative (ENG) and DNG materials. Also, especially, in configurations that exhibit spatial dispersion (i.e. a dependence of the permittivity or permeability on the wavevector, $\epsilon(\omega, k)$ and $\mu(\omega, k)$) [26–28].

1.4.2 Artificial Magnetic Media

Research into artificial magnetic media dates back to the work of Schelkunoff and Friis [29] in the 1950s and the proposed Split Ring Resonator (SRR). Engineered high-permeability materials are especially interesting as most conventional materials of the magnetic field component of the EM wave couples only weakly to the material [30]. Magnetism without magnetic materials has been known for sometime, such as "wet" ice crystals, where the water in the system causes a diamagnetic behavior, although even in these systems, the relative permeability is low. Today, the SRR remains the magnetic meta-atom of choice for researchers, although multiple researchers have examined the SRR in depth (see for example [31, 32]), the basic geometry remains the same as that originally proposed by Schelkunoff in 1950.

Figure 1.3 (a) Double SRR geometry building block, and (b) An array of SRRs. (c) The equivalent circuit diagram from the SRR shown in (a).

Due to the significance of the SRR, it is pertinent to review the key aspects of its function and behavior. Consider the geometry shown in Figure 1.3, a double SRR formed from concentric metallic tracks similar to the design of Pendry et al. [33]. We consider the case where this SRR meta-atom is much smaller than the wavelength of interest allowing a system of multiple SRRs to be described by effective medium theory. At the level of an individual meta-atom, the incident wave upon a SRR produces a magnetic flux to oppose the incident field. Without the split, this interaction would be purely an inductive nonresonant phenomena, resulting in a weakly diamagnetic system. The split prevents the current circulating causing a collection of charge at the split edge creating a capacitance.

A meta-atom with a single SRR will accumulate charge at the gap creating a large electric dipole moment that in most cases dominate over the magnetic dipole moment. A second concentric SRR where the "gaps" of the SRRs are opposite each other offers control over the capacitance of the meta-atom, allowing the electric dipole moment of the inner ring to suppress the electric dipole moment of the outer ring, allowing the magnetic moment to dominate the system.

The resulting SRR configuration can be modeled as an equivalent subwavelength quasi-static LCR circuit, shown in Figure 1.3. This circuit although a crude first approximation can present great insights into the system's response and behavior of the artificial material over all. The inductive elements of the equivalent circuit are relatively easy to determine, estimated by $L \approx 2\mu_0 r$. The Ohmic loss in the system can be estimated as $R \approx \pi r/c\sigma\delta$. Determining the capacitance is tricky as in addition to the capacitive effects of the split "gaps," there is also the capacitance from the gap that separates the two SRRs. An analysis conducted by Baena et al. [34] approximates the capacitance of the double SRR system by $C \approx \pi r \epsilon_0 t/2d$, where t is the combined width of the rings and d the separation between the rings. This enables the resonant frequency of the meta-atom to be estimated as $\omega_0 = \sqrt{1/(L + R/j\omega_0)C}$. Using the resonant frequency, we can estimate, to first order, the magnetic moment m_h of an individual meta-atom in response to an incident wave of magnetic field, H [35]:

$$m_h(\omega) = \frac{\pi^2 r^4 \mu_0 H}{(\omega_0^2/\omega^2 - 1)L}. \tag{1.3}$$

Using Eq. (1.3) one can then determine the effective permeability [35] (μ_{eff}) of an artificial material formed from a lattice of individual subwavelength SRRs:

$$\mu_{\text{eff}}(\omega) = 1 + \frac{m_h}{VH}. \tag{1.4}$$

V is the unit-cell volume for an individual meta-atom. This approach is of course rather crude and does not take into account electric coupling or the bianisotropic nature of the material. Although it does enable us, at least to first order, to gain useful insights into how engineered changes to the unit-cell geometry will alter the effective permeability of our artificial material.

1.5 Double Negative Media

Although several researchers have considered materials with simultaneous negative permittivity and permeability (DNG materials) [36], and materials with a negative index of refraction [37] prior to 1965. The first systematic study of the general properties of a hypothetical DNG medium with a negative refractive index is attributed to the seminal 1967 paper by Veselago [38]. In this paper, Veselago examined plane-wave propagation in a material with simultaneous negative permittivity and permeability. His theoretical study showed that a monochromatic uniform plane wave propagating in such a medium in the direction of the Poynting vector would be antiparallel to the direction of the phase velocity, contrary to the case of plane wave propagation in conventional simple media. Veselago then considered the possibility of a lens constructed from this material.

The refractive index (n) is one of the most important parameters used to describe the propagation of EM waves across a medium, where in general n has a complex frequency dependent form $n = n' + jn''$. The real component relates to the phase velocity of the wave and the imaginary component the extinction coefficient of the medium. Where the refractive index is related to the constitutive relations by

$$n = \sqrt{\epsilon\mu}. \tag{1.5}$$

If we consider the case of simultaneous negative permittivity ($\epsilon = -1 + ja$) and permeability ($\mu = -1 + jb$), then Eq. (1.5) yields

$$n = \pm\left[1 - j(a + b)\right]. \tag{1.6}$$

To preserve causality, the imaginary component of n must be greater than zero, but there is no restriction on the sign of the real component. Hence, in the case of both permittivity and permeability are negative, the refractive index is also negative. Materials where the real component of the refractive is less than zero are often referred to as Negative-Index Materials (NIMs). The most obvious impact of a NIM is the effect on Snell's law ($n_1 \sin\theta_1 = n_2 \sin\theta_2$), where an EM wave incident on a NIM is refracted to the same side, of the normal to the interface, to the incident EM wave, as seen in Figure 1.6(B)c. To consider the impact of a medium consisting of simultaneous negative permittivity and permeability Veselago considered the effect directly from Maxwell's equations:

$$\begin{aligned} \nabla \times \mathbf{H} &= j\omega\epsilon\mathbf{E} \\ \nabla \times \mathbf{E} &= -j\omega\mu\mathbf{H}. \end{aligned} \tag{1.7}$$

Assuming a plane wave of the form $\exp j(\mathbf{k} \cdot \mathbf{r} - \omega t)$ propagating through the medium then from Eq. (1.7) we have

$$\begin{aligned} \mathbf{k} \times \mathbf{H} &= \omega\epsilon\mathbf{E} \\ \mathbf{k} \times \mathbf{E} &= -\omega\mu\mathbf{H}. \end{aligned} \tag{1.8}$$

The impact of a simultaneous negative ϵ and μ on both $\mathbf{H}$ and $\mathbf{E}$, and on the wave vector k can be seen from Eq. (1.8). As $\mathbf{k}$ gives the direction of the phase velocity $v_p = n/c = \omega/\mathbf{k}$, and the Poynting vector ($\mathbf{E} \times \mathbf{B}$) gives the direction of the group velocity v_g. Hence, in the case of simultaneous negative ϵ and μ, the "energy" propagates in the opposite direction to k. Veselago coined the term "Left-Handed Materials (LHMs)" for such media because the field vectors E, H, and wavevector k form a "left-handed system," as opposed to the "right-handed system" formed by conventional materials. Although we know this "left-handed" property is known to occur in multiple systems not just in DNG media.

Veselago [38] also discussed several remarkable properties that would derive from a DNG medium, such as the reversed Doppler effect, where a detector in a DNG medium moving toward

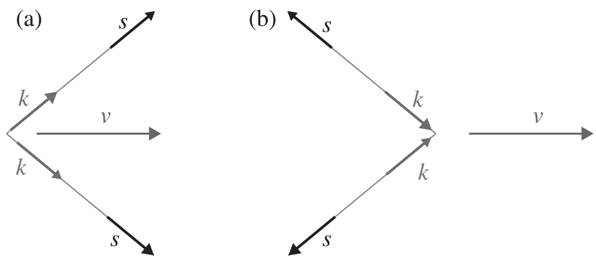

Figure 1.4 (a) Cerenkov effect in a DPM, (b) The same effect in a DNG material. Where v is the particle velocity, S the Poynting vector, and k the wave vector.

a source which emits a frequency ω_0 will detect a frequency ω that is smaller than ω_0, not larger as would be the case in a right-handed medium. Although one of the most interesting phenomena, from the point of view of HPM VEDs, is the reversed Vavilov–Cerenkov effect. A particle moving though a medium with speed v in a straight line, as shown in Figure 1.4, will emit EM radiation according to $\exp i(k_z z + k_r r - \omega t)$. k_z is the wavevector component in the direction of the beam, and k_r is the wavevector component perpendicular to the beam. The wavevector of the emitted EM radiation from the moving particle is $k' = k_z / \cos\theta$ and is in the general direction of the particle velocity v. Where the k_r component is media-dependent and given by

$$k_r = p \left| \sqrt{k'^2 - k_z^2} \right|. \tag{1.9}$$

The choice of sign in Eq. (1.9) ensures that the energy moves away from the radiating particle to infinity and the angle θ of the Cherenkov radiation cone is given by $\cos\theta = (n\beta)^{-1}$, where β is the normalized particle velocity. Hence, for a DNG with $n < 0$ the Cherenkov radiation will be "backward" as the angle θ is obtuse, as shown in Figure 1.4.

The seminal paper by Pendry [5] in 2000 marked a turning point for artificial materials and can be said to be the key driver for the tremendous increase in interest and research of artificial materials since the beginning of the twenty-first century. The key aspect of Pendry's paper was to reconsider the Veselago lens using transformative optics and presenting the mechanism that allows the diffraction limit to be beaten. Pendry pointed out how evanescent waves propagating in a DNG material can be redistributed in space so that the waves are transported far from the source [5]. Importantly in earlier work Pendry et al. [33] presented and discussed the key subwavelength elements that could be used to construct a DNG material unit-cell. These elements were the double SRR to control the permeability and wire array to control the permittivity.

The first realizations of DNG materials came from the work by Smith and Schultz who constructed the first DNG media in 2000–2001. The basic form realized was a material with a negative refractive index in one direction of propagation [39]. This work was quickly followed by the famous two-dimensional NIM paper [6], where each subwavelength unit cell consists of two basic elements, a double SRR supported on a dielectric substrate (FR4) with a Cu track (wire) placed uniformly between the split rings on the opposite side of the FR4. The subwavelength component elements were tailored to give a specific EM response over a certain frequency range, the wire array was used to give an effective negative permittivity and the SRR to give a negative effective permeability. In the paper [6], Smiths group demonstrated the NIM behavior of the above material by performing an experimental measurement using Snell's law, where the materials were shaped into a wedge to form a prism. The experiment was performed at 10.5 GHz with the RF propagating in parallel plate system with microwave absorber on each side to produce plane waves incident on to the back of the

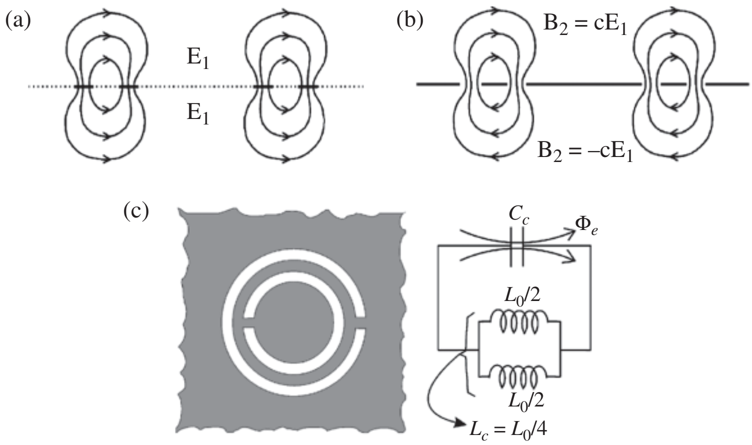

Figure 1.5 (a) Electric field lines in the SRR at resonance. (b) Magnetic field lines in the dual CSRR. (c) CSRR and the equivalent-circuit models, grey represent the metal areas. Diagrams taken from the paper [41].

prism. The results showed that the EM wave propagating through the DNG media was refracted though an angle of −61°, corresponding to a material with a refractive index of −2.7.

1.5.1 DNG Realization

One of the most common approaches to realizing a DNG media is a combined meta-atom consisting of an SRR to give the negative permeability response, and a conducting wire strip acting as a shunt inductance, creating a wire array throughout the material that presents a negative permittivity. This configuration does require a way to support the two elements electrical succinct from each other usually achieved by using a dielectric substrate between wire strip line and SRR. Although, of course, the use of a dielectric substrate does lead to additional loss in the unit cell which in a VED can have devastating impact. An alternative approach developed by Falcone et al. [40] is to derive a planar negative of the SRR in metal, this complementary SRR or CSRR is shown in Figure 1.5, where the gaps cutting into the metal are the complement of the SRR tracks. In terms of operation, the capacitances of the SRR are replaced by inductors in the CSSR. The result is that the CSSR presents a negative permittivity response to an incident EM wave. The CSRR exhibits an electromagnetic behavior which is almost the dual of that of the SRR. Recently a range of other geometries have been used to construct DNG unit-cells, such as the electromagnetically induced transparency geometries [42].

1.6 Backward Wave Propagation

The concept of backward wave propagation in materials and structures is of course well known to microwave engineers through the theory of backward-wave VEDs developed by Brillouin [43] and Pierce [44] in the late 1940s. Pierce's theory of traveling-wave interactions assumes a slow-wave circuit in which two waves propagate, one forward wave and one backward wave. This interaction can be modeled via an equivalent circuit model of series-capacitance/shunt-inductance [44]. This research sparked a vast body of work around 1D structures as slow-wave periodic systems for applications in VEDs [45], and this approach is the cornerstone of many commercial devices.

The possibility and consequences of materials with negative group velocity has been considered by researchers as far back as 1904 in the work of Schuster and Lamb [37, 46]. Schuster discussed

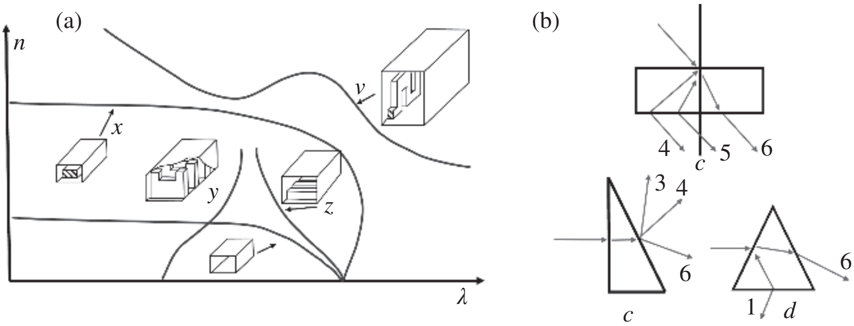

Figure 1.6 The dispersion relation for various waveguide loaded artificial dielectrics (a). Positive and negative refraction in artificial dielectrics (b). Figure created by R. Seviour based on Figure 1 from [49]. (a) x: Material with both positive and negative dispersion, y: Negative media, v: Positive media with anomalous dispersion. (b) 1: $n < 0$, 2: $n > 0$, 3: $n < -1$, 4: $-1 < n < 0$, 5: $n < -1$, 6: $n > 1$. Source: Silin [50].

that in the region of an absorption band as the wavelength decreases, the wave velocity increases, and the group and phase velocity can be anti-parallel [37]. Schuster used this concept to consider an EM wave incident on an isotropic semi-infinite block of backward wave material. Schuster noted that "the wave entering such a medium is greater than the angle of incidence," concluding that energy can be carried forward by the group velocity but in the opposite direction to the phase velocity. In this case, the observed negative refraction is clearly linked to the negative phase velocity due to anomalous dispersion without the need to invoke the concept of negative permittivity or permeability.

In contrast, Lamb [47] considered acoustic wave propagation in a fictitious 1D medium, examining the relationship between group and phase velocities of the waves. The work of Lamb and Schuster paved the way for the seminal paper by Mandelstam [48], who noted that in a medium with negative dispersion, a wave's group velocity is in the opposite direction to the k vector. This led to his conclusion that negative refraction would occur at an interface with such a medium. In Schuster's Work, negative refraction is clearly linked to negative phase velocity, although in general, it is not necessary to associate backward wave propagation with negative refraction [49].

The 1972 paper by Silin [50] presents an excellent review of waveguides loaded with various artificial materials. Silin examined multiple materials that exhibited a range of properties: positive and negative dispersion, negative index of refraction, and backward wave propagation (shown in Figure 1.6). The left-hand side of Figure 1.6, curve 4, shows a system where a segment of the dispersion curve exhibits positive anomalous dispersion. Silin discussed that unlike conventional dielectrics, artificial-dielectrics can exhibit anomalous dispersion even when losses are neglected [50]. Silin also points out that for artificial dielectrics with a multivalued dispersion curve (Figure 1.6, curve X) birefringence can arise. Critically, none of the structures presented in Silin's review are DNG materials. The first researcher to consider backward wave propagation in materials arising from simultaneous negative permittivity and permeability was Sivukhin [36] in 1957, where he noted that no material with simultaneous negative permittivity and permeability was known.

1.7 Dispersion

Artificial materials offer many unusual and promising features, derived primarily from their structure rather than their composition. Among these unusual properties are negative refraction, backward Cherenkov radiation, and surface waves propagating at the interface with an ordinary material. One feature in particular that makes MTMs very attractive for HPM VEDs is the ability to arbitrarily engineer the dispersion relation of the material [51], enabling engineers to create materials that produce EM waves with very low-group velocities (i.e. SWS), thus ensuring that we can synchronize a beam with an EM wave. These unusual electrodynamic properties make MTMs an excellent choice for use in VEDs.

To investigate the ability to tailor the dispersion relation of these materials, we start from the Lorentz model for a bulk, isotropic, homogeneous material, where electron motion in the material is described in terms of a driven, dampened, harmonic oscillator. The Lorentz model describes the temporal response of the polarization field of the material to the EM field via the second order PDE

$$\frac{d^2}{dt^2}P_i + \Gamma_L \frac{d}{dt}P_i + \omega_0^2 P_i = \epsilon_0 \chi_L E_i, \tag{1.10}$$

where the first term represents an acceleration force, the second term accounts for dampening via the dampening coefficient Γ_L, and the third term is a restorative force. The driving term on the RHS couples to the system via χ_L. Equation (1.10) also enables us to gain an insight into the frequency-dependent behavior of our DNG material by considering a mechanical analogy of a mass on a spring, looking at the effect of the driving and damping forces. Equation (1.10) also allows us to describe the material response to an EM wave via a dispersive Drude (effective permittivity) and Lorentz (effective permeability) model, deriving expressions for the effective permittivity (ϵ_f) and permeability (μ_f):

$$\epsilon_f(\omega) = \epsilon_\infty - \frac{\epsilon_\infty \omega_p^2}{\omega(\omega - j v_c)},$$
$$\mu_f(\omega) = \mu_\infty + \frac{(\mu_s - \mu_\infty)\omega_0^2}{\omega_0^2 - \omega^2 + j\omega\sigma}. \tag{1.11}$$

In general ϵ_f and μ_f are complex dispersive parameters, where the real components relate the response of the material to the incident EM wave, and the imaginary component relates to the loss component of the EM wave. Here, ϵ_∞ is the permittivity in the high-frequency limit, ω_p is the radial plasma frequency, v_c is the collision frequency, μ_s (μ_∞) is the permeability at the low(high)-frequency limit, ω_0 is the radial resonant frequency, and σ is the damping frequency. Figure 1.7(a) shows the real components of the effective permittivity and permeability calculated using Eq. (1.11) for a bulk block of artificial material as a function of frequency. As seen in Figure 1.7(a), there is a "narrow" frequency range between 9.5 and 10.5 GHz where the material behaves as a DNG; this relatively narrow band frequency range where the media behaves as a DNG is common for media constructed using SRRs. Outside of this narrow frequency range the bulk material behaves as a single negative media, meaning wave transport occurs evanescently.

The more relevant case for HPM VED applications isn't bulk media in vacuum, but media loaded into a waveguide type geometry. Several authors have made use of loading waveguides below cutoff with artificial media, to provide an additional material parameter, i.e. a waveguide below cutoff behaves as a plasma, which is a negative permittivity media. For the example here, we have chosen WR102 waveguide (similar to [51]), operated above cutoff between 7 and 11 GHz and loaded with the material with the parameters shown in Figure 1.7(a). In the case where we have a dielectric loaded waveguide, the propagation constant β for the TE_{10} mode is given by

$$\beta = \sqrt{\frac{\omega^2 \epsilon_f \mu_f}{c} - \frac{\pi^2}{a^2}}. \tag{1.12}$$

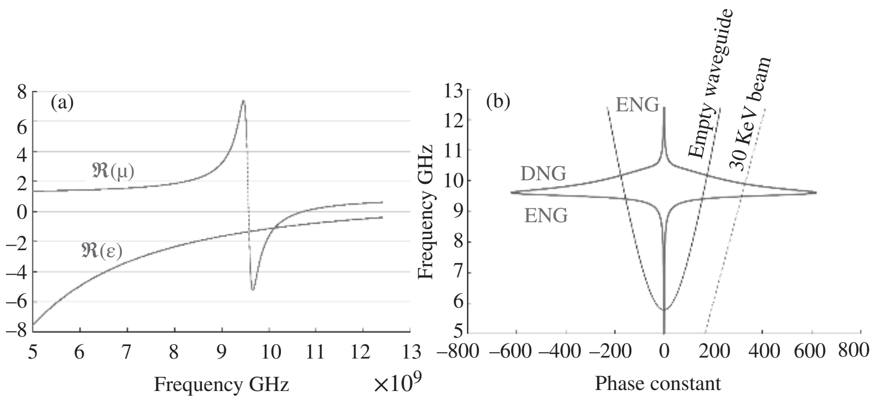

Figure 1.7 (a) The real components of ϵ_{eff} and μ_{eff} calculated via Eq. (1.11), using the following material parameters; $\epsilon_{\infty=1.12}$, $\omega_p = 2\pi 3.62 \times 10^7$, $\upsilon_c = 3.07 \times 10^7$, $\mu_s = 1.26$ (μ_∞, $\sigma = 1.24 \times 10^9$ and $\omega_0 = 2\pi 9.56 \times 10^9$. (b) the dispersion for an empty waveguide and waveguide loaded with the material from (a), also showing the beam line for a 30 keV electron beam. Source: (a) Based on Silin [50].

ϵ_f and μ_f are determined from Eq. (1.11) as shown in Figure 1.7(a), and a is the dimension of the WR102 waveguide (defining the cutoff frequency). The dispersion for this system is shown in Figure 1.7(b), the black curve shows the dispersion for an empty WR102 waveguide. The dashed line shows the 30 keV beamline. The dispersion for the WR102 waveguide loaded with our "metamaterial" is more complicated; in different regions of the dispersion curve the system behaves either as a DNG system, or as a single negative system.

Figure 1.7(b) also shows several interesting turning points, which if we use the definition for the group velocity $\upsilon_g = d\omega/dk$ seems to imply a velocity greater than c, although we have to remember the definition of group velocity $\upsilon_g = d\omega/dk$ is only true for a nondispersive or at best a weakly dispersive media. DNG materials by their very nature are dispersive media and, in the regions of these cusps, are highly dispersive to the point that the group velocity is not well defined. The key point to take from Figure 1.7(b) is that the inclusion of the artificial material engineers the dispersion to enter a regime where the empty waveguide could not reach. Specifically, the material, when acting as a DNG, has a negative dispersion curve and has an interaction point with a relatively low-voltage electron beam. The results of Figure 1.7 show that artificial materials can be used to tailor a dispersion relation to maximize and control the interaction between wave and beam, presenting a very powerful tool for the design and development of HPM VEDs.

1.8 Parameter Retrieval

As discussed, theoretical approaches to predicting the behavior of artificial materials can give us great insight into how a particular material configuration will function to first order, although for a technological application, it is crucial to understand how a specific material actually functions. In this section, we examine how to determine the material's effective permittivity and permeability from measurements of the scattering parameters.

In the literature, there are a number of papers on how to determine the permittivity and permeability of MTMs from S-parameter measurements. Nearly all of these methods are rooted in the standard Nicolson-Ross-Weir (NRW) technique [52, 53], the accepted standard technique for measuring the complex permittivity and permeability of homogeneous, isotropic materials. The key point to this formalism is that the NRW uses a closed-form expression allowing the complex form of the permittivity and permeability to be determined directly from S-parameter measurements. In addition, the NRW technique is relatively robust to experimental error. Although positioning the material to a calibrated phase point in an experiment is easier said than done.

The approach presented here is a variant of the NRW approached adapted by Smith et al. [54] to account for possible negative responses in the real components of the permittivity and permeability. The technique is relatively straight forward but does require an understanding of the physics involved to ensure the correct solutions are selected. The approach starts from the assumptions that the media is in the form of a free-standing slab surrounded by a vacuum, with normal incident plane waves. If we consider a slab of material, thickness d, then the S-parameters S_{21} and S_{11} of the wave from the slab are given by

$$S_{21} = \left[\cos(nkd) - \frac{j}{2}\left(Z + \frac{1}{Z}\right)\sin(nkd)\right]^{-1}, \tag{1.13}$$

$$S_{11} = -\frac{j}{2}\left(Z - \frac{1}{Z}\right)\sin(nkd) \cdot S_{21}. \tag{1.14}$$

$k = 2\pi/\lambda_0$ is the free space wave vector, $Z = Z' + jZ''$ the impedance of the material, and $n = n' + n''$ the refractive index. By inverting 1.13 an 1.14, we can find expressions for the impedance Z and refractive index n in terms of the known quantities:

$$Z = \pm\left[\frac{(1+S_{11})^2 - S_{21}^2}{(1-S_{11})^2 - S_{21}^2}\right]^{1/2}, \tag{1.15}$$

$$n' = \pm\frac{1}{kd}\mathrm{Re}\left[\cos^{-1}\left(\frac{1 - S_{11}^2 + S_{21}^2}{2S_{21}}\right)\right] + \frac{2\pi m}{kd}, \tag{1.16}$$

$$n'' = \pm\frac{1}{kd}\mathrm{Im}\left[\cos^{-1}\left(\frac{1 - S_{11}^2 + S_{21}^2}{2S_{21}}\right)\right], \tag{1.17}$$

where m is an integer. Once Z and n have been determined the permittivity and permeability can be determined directly from $\epsilon_f = n/Z$ and $\mu_f = nZ$. The tricky part is of course to choose the correct root and branch of Eqs. (1.15), (1.16), and (1.17) to give the correct solutions for Z and n. To ensure causality is maintained for a passive media the imaginary components of ϵ_f, μ_f, n and the real component of Z must be positive (except at points of anti-resonances). The inverse cosine function in n introduces some ambiguity, as although the real component is bound between 0 and π, the imaginary component remains unconstrained. The second condition is to select the correct solution branch of Eq. (1.16) by choosing the correct m to ensure that n' is continuous across the frequency range. For convenience, it is best to start at a frequency far from any resonances in the material, meaning m starts at the 0th branch.

1.9 Loss

As discussed in Section 1.4.2, DNG materials consist of resonant elements where the operation of the material at resonance is necessary to achieve a DNG response. This results in a relatively high field near the metal components of the unit-cell. This has led several authors to claim that due to unavoidable losses and dispersion, DNG materials would not be usable [55, 56]. Ohmic loss due to current flow in the metallic elements of the unit-cell can becomes the dominant loss mechanisms in DNG materials especially at high frequencies. Ohmic loss due to the constituent materials of the meta-atoms is not the only cause of loss, but EM field concentration in the resonant elements and nonuniform current due to the geometry of the unit-cells can dominate the loss process [57]. This has motivated several authors to consider reducing losses by tailoring the geometry of the unit-cells [58, 59]. The high-level of loss exhibited naturally from DNG materials has led some authors to propose novel technologies that capitalize on this loss for a beneficial end, such as novel absorber materials [60].

1.10 Summary

This book seeks to introduce the reader to the use of MTMs and DBE structures for dispersion engineering to identify novel beam/wave interactions in the quest for new classes of HPM amplifiers. Chapter 2 summarizes recent advances toward using multitransmission line models to discuss beam/wave interactions. Chapter 3 describes a self-consistent derivation of the Pierce model from a Lagrangian formulation. Chapter 4 summarizes dispersion engineering uses and cold tests of DNG MTM SWSs, DBE structures, as well as other novel structures. Chapter 5 describes a perturbation analysis of Maxwell's Equations to describe beam/wave interactions. Chapter 6 reviews recent work that shows that the properties thought to be unique to MTM structures appear in conventional metallic periodic structures with deep corrugations. Chapter 7 summarizes the novel use of group theory in designing passive MTM structures for HPM applications. Chapter 8 reviews recent advances in the understanding of the time-domain response of MTM structures in the microwave regime. Chapter 9 reviews recent work on the survivability of MTM structures in the HPM environment. Chapter 10 reviews recent experimental hot tests of MTM and DBE SWSs. The conclusions and future directions for this research are presented in Chapter 11.

References

1 Barker, R.J. and Schamiloglu, E. (2001). *High-Power Microwave Sources and Technologies*. IEEE Press/Wiley.
2 Benford, J., Swegle, J., and Schamiloglu, E. (2016). *High Power Microwaves*, 3e. CRC Press.
3 Korovin, S.D., Rostov, V.V., Polevin, S.D. et al. (2004). Pulsed power-driven high-power microwave sources. *Proc. IEEE* 92: 1082.
4 Gewartowski, J.W. and Watson, H.A. (1965). *Principles of Electron Tubes: Including Grid-Controlled Tubes, Microwave Tubes, and Gas Tubes*. Van Nostrand.
5 Pendry, J.B. (2000). Negative refraction makes a perfect lens. *Phys. Rev. Lett.* 85: 3966.
6 Shelby, R.A., Smith, D.R., and Schultz, S. (2001). Experimental verification of a negative index of refraction. *Science* 292: 77–79.
7 Capolino, F. (2009). *Theory and Phenomena of Metamaterials*. CRC Press.
8 Cai, W. and Shalaev, V. (2010). *Optical Metamaterials: Fundamentals and applications*. Springer.
9 Munk, B.A. (2009). *Metamaterials: Critique and Alternatives*. Wiley.
10 Metamorphose VI AISBL. The virtual institute for artificial electromagnetic materials and metamaterials. http://www.metamorphose-vi.org/index.php/metamaterials (accessed 02 June 2018).
11 Bryceson, K. (1981). Focusing of light by corneal lens in a reflecting superposition eye. *J. Exp. Biol.* 90: 347–350.
12 Mossotti, O.F. (1850). Sobre las fuerzas que rigen la constituciòn de los cuerpos. *Memorie di Matematica e di Fisica della Societä Italiana delle Scienze Residente in Modena* 24 (2): 49–74.

13 Clausius, R. (1879). *Die Mechanische Wärmtheorie*. Vieweg.

14 Lakhtakia, A. (1996). *Selected Papers on Linear Optical Composite Materials*. SPIE Press.

15 Belov, P. and Simovski, C. (2005). Homogenization of electromagnetic crystals formed by uniaxial resonant scatterers. *Phys. Rev. E* 72: 1–9.

16 Maxwell-Garnett, J.C. (1904). Colours in metal glasses and in metallic films. *Philos. Trans. R. Soc. London* 203: 385–420.

17 Bruggeman, D.A.G. (1935). Berechnung verschiedener physikalischer konstanten von heterogenen substanzen. i. dielektrizitätskonstanten und leitfähigkeiten der mischkörper aus isotropen substanzen. *Ann. Phys.* 416 (7): 636–664.

18 Rayleigh, L.R.S. (1892). On the influence of obstacles arranged in rectangular order upon the properties of a medium. *The London, Edinburgh, and Dublin Philos. Mag. J. Sci.* 5 (34): 481–502.

19 Bose, J.C. (1898). On the rotation of plane of polarisation of electric wave by a twisted structure. *Proc. R. Soc. London* 63: 146–152.

20 Lindman, K.F. (1914). Om en genom ett isotropt system av spiralformiga resonatorer alstrad rotationspolarisation av de elektro-magnetiska vagorna. *Öfversigt af Finska Vetenskaps-Societetens Förhandlingar* A LVII: 1–32.

21 Kock, W.E. (1948). Metallic delay lenses. *Bell Syst. Tech. J.* 27: 58.

22 Brown, J. (1953). Artificial dielectrics having refractive indices less than unity. *J. Proc. IEEE* 100 (5): 51–62.

23 Kharadly, M.M.Z. and Jackson, W. (1962). The properties of artificial dielectrics comprising arrays of conducting elements. *Proc. IEE* 100: 199.

24 Rotman, W. (1962). Plasma simulation by artificial dielectric and parallel-plate medial. *IRE Trans. Anntenas Propag.* 10 (1): 82–95.

25 Chekroun, C., Herrick, D., Michel, Y.M., Pauchard, R., Vidal, P. (1979). Radant—New method of electric scanning. *L'Onde Electr.* 59 (89): 89–94.

26 Belov, P.A., Marqués, R., Maslovski, S.I., Nefedov, I.S., Silveirinha, M., Simovski, C.R., Tretyakov, S.A. (2003). Strong spatial dispersion in wire media in the very large wavelength limit. *Phys. Rev. B* 67: 113103.

27 Boyd, T., Gratus, J., Kinsler, P., and Letizia, R. (2018). Customizing longitudinal electric field profiles using spatial dispersion in dielectric wire arrays. *Opt. Express* 26: 2478–2494.

28 Gratus, J. and McCormack, M. (2015). Spatially dispersive inhomogeneous electromagnetic media with periodic structure. *J. Opt.* 17: 2040–8978.

29 Schelkunoff, S.A. and Friis, H.T. (1952). *Antennas: Theory and practice*. Wiley.

30 Landau, L., Liftshitz, E., and Pitaevskii, L. (1984). *Electrodynamics of Continuous Media*. Pergamon.

31 Hardy, W.N. and Whitehead, L.A. (1981). Split-ring resonator for use in magnetic resonance from 200–2000 MHz. *Rev. Sci. Instrum.* 52: 213–216.

32 Schneider, H.J. and Dullenkopf, P. (1977). Slotted tube resonator: a new NMR probe head at high observing frequencies. *Rev. Sci. Instrum.* 48: 68.

33 Pendry, J.B., Holden, A.J., Robbins, D.J., and Stewart, W.J. (1999). Magnetism from conductors and enhanced nonlinear phenomena. *IEEE Trans. Microwave Theory Tech.* 47: 2075–2084.

34 Baena, J.D., Marques, R., Medina, F., and Martel, J. (2004). Artificial magnetic metamaterial design by using spiral resonators. *Phys. Rev. B* 69: 014402.

35 Marques, R., Medina, F., and Rafii-El-Idrissi, R. (2002). Role of bianisotropy in negative permeability and left-handed metamaterials. *Phys. Rev. B* 65: 144440.

36 Sivukhin, D.V. (1957). The energy of electromagnetic waves in dispersive media. *Opt. Spektrosk.* 3: 308.

37 Schuster, A. (1904). *An Introduction to the Theory of Optics*. London: Edward Arnold.
38 Veselago, V.G. (1967). The electrodynamics of substances with simultaneously negative values of ϵ and μ. *Usp. Fiz. Nauk* 92: 517–526.
39 Smith, D.R., Padilla, W.J., Vier, D.C., Nemat-Nasser, S.C., Schultz, S. (2000). Composite medium with simultaneously negative permeability and permittivity. *Phys. Rev. Lett.* 84: 4184–4187.
40 Falcone, F., Lopetegi, T., Baena, J.D. et al. (2004). Effective negative-ϵ stopband microstrip lines based on complementary split ring resonators. *IEEE Microwave Wireless Compon. Lett.* 14: 280.
41 Baena, J.D., Bonache, J., Martín, F., Sillero, R.M., Falcone, F., Lopetegi, T., Laso, M.A.G., García-García, J., Gil, I., Portillo, M.F., Sorolla, M. (2005). Equivalent circuit models for split-ring resonators and complementary split-ring resonators coupled to planar transmission lines. *IEEE Microwave Wireless Compon. Lett.* 53: 1461.
42 Liao, Z., Liu, S., Ma, H.F., Li, C., Jin, B., Cui, T.J. (2016). Electromagnetically induced transparency metamaterial based on spoof localized surface plasmons at terahertz frequencies. *Sci. Rep.* 6: 27596.
43 Brillouin, L. (1946). *Wave Propagation in Periodic Structures*. McGraw-Hill.
44 Pierce, J.R. (1950). *Traveling-Wave Tubes*. Van Nostrand.
45 Altman, J.L. (1964). *Microwave Circuits*. Van Nostrand.
46 Lamb, H. (1904). On group-velocity. *Proc. London Math. Soc.* 1: 473–479.
47 Lamb, H. (1916). *An Introduction to the Theory of Optics*. Cambridge: University Press.
48 Mandelshtam, L. (1945). Group velocity in a crystal lattice. *Zh. Eksp. Teor. Fiz.* 15: 475–478.
49 Boardman, A.D., King, N., and Velasco, L. (2005). Negative refraction in perspective. *Electromagnetics* 25 (5): 365–389.
50 Silin, R.A. (1972). Optical properties of dielectrics (review). *Radiofizika* 15 (6): 809–820.
51 Tan, Y. and Seviour, R. (2009). Wave energy amplification in a metamaterial based traveling wave structure. *Europhys. Lett.* 87: 34005.
52 Nicolson, A.M. and Ross, G.F. (1970). Measurement of the intrinsic properties of materials by time domain techniques. *IEEE Trans. Instrum. Meas.* 19 (4): 377–382.
53 Weir, W.B. (1974). Automatic measurement of complex dielectric constant and permeability at microwave frequencies. *Proc. IEEE* 62 (1): 33–36.
54 Smith, D.R., Vier, D.C., Koschny, T., and Soukoulis, C.M. (2005). Electromagnetic parameter retrieval from inhomogeneous metamaterials. *Phys. Rev. E* 71: 036617.
55 Garcia, N. and Nieto-Vesperinas, M. (2002). Is there an experimental verification of a negative index of refraction yet? *Opt. Lett.* 27: 885.
56 Dimmock, J. (2003). Losses in left-handed materials. *Opt. Lett.* 11: 2397.
57 Seviour, R., Tan, Y.S., and Hopper, A. (2014). Effects of high power on microwave metamaterials. *2014 8th International Congress on Advanced Electromagnetic Materials in Microwaves and Optics*, pp. 142–144.
58 Hopper, A. and Seviour, R. (2016). Wave particle cherenkov interactions mediated via novel materials. *Proceedings of International Particle Accelerator Conference (IPAC'16)*, Busan, Korea, May 8–13, 2016, pp. 1960–1962.
59 Koschny, T., Zhou, J., and Soukoulis, C.M. (2007). Magnetic response and negative refractive index of metamaterials. *Proceedings of SPIE 6581, Metamaterials II*, p. 658103.
60 Landy, N., Sajuyigbe, S., Mock, J.J. et al. (2008). Perfect metamaterial absorber. *Phys. Rev. Lett.* 100: 207402.